Materials Science & Engineering A 649 (2016) 449–460

Contents lists available at ScienceDirect

Materials Science & Engineering A

journal homepage: www.elsevier.com/locate/msea

Size-dependent plastic deformation and failure mechanisms of nanotwinned Ni_3Al: Insights from an atomistic cracking model

Yun-Jiang Wang [a,*], Koichi Tsuchiya [b], L.H. Dai [a,**]

[a] State Key Laboratory of Nonlinear Mechanics, Institute of Mechanics, Chinese Academy of Sciences, Beijing 100190, China
[b] Research Center for Strategic Materials, National Institute for Materials Science, 1-2-1 Sengen, Tsukuba, Ibaraki 305-0047, Japan

ARTICLE INFO

Article history:
Received 7 September 2015
Received in revised form
1 October 2015
Accepted 3 October 2015
Available online 9 October 2015

Keywords:
Nanostructured materials
Twinning
Crystal plasticity
Fracture
Atomistic simulations

ABSTRACT

The polycrystalline Ni_3Al is brittle since the notorious intergranular fracture mode hinders its applications. Here we perform molecular dynamics to highlight the unique role of nanotwin boundary in the plastic deformation and failure mechanisms of Ni_3Al via an atomistic cracking model. Surprisingly, the strength, ductility and fracture toughness of the nanotwinned Ni_3Al are revealed to increase simultaneously with reducing twin size, possibly evading a traditional tradeoff between ductility/toughness and strength. A possible quasi-brittle fracture mode in single crystalline Ni_3Al is recognized as nucleating twinning partials from crack tip. However, the pre-existing twin boundaries can suppress the emission and propagation of successive twinning dislocations. Instead, dislocation avalanches happen and serve as a crack blunting mechanism which leads to the ductile fracture pattern of the nanotwinned Ni_3Al. A size-dependent transition of fracture mode from dislocation nucleation to shear localization is observed as twin becomes very small. A physical model combined with energetics analysis is provided to rationalize the transition. Our atomistic insights are in qualitative agreement with recent observations of improved strength and ductility of Ni_3Al with disordered nanotwinned structure after severe plastic deformation.

1. Introduction

Nickel aluminides are a category of intermetallic alloys composed of nickel and aluminum which present mechanical properties similar to both metallic materials and ceramics [1]. This is because of the covalent-like metallic bonding between Ni and Al [2–4]. Among them, the $L1_2$ (face-centered cubic, with Ni on the face and Al on the corner) structured Ni_3Al exhibits extraordinary elevated-temperature properties and it is potentially served as an ideal creep resistance material [5]. The long-range ordered superlattice of $L1_2$ structure can effectively suppress the diffusive processes and dislocation mobilities, therefore, leads to the high strength of Ni_3Al even at elevated temperatures. Probably the most well-known utility of Ni_3Al is that it is frequently used as a strengthening constituent (γ' phase) of the single-crystalline nickel-based superalloys [1]. Combined its high thermal conductivity, low density, and unique high-temperature strength, the Ni-base superalloys have been widely used in aerospace and power industries [1]. But there exist obvious disadvantages of the pristine Ni_3Al.

Even though Ni_3Al has very high theoretical strength [4] and exhibits superior high-temperature performances, there remains a long-standing bottleneck of its applications as structural materials. The unalloyed polycrystalline Ni_3Al itself is notorious for its brittle fracture manner since the intergranular fracture [6,7]; see an example of $\Sigma 7$ grain boundary fracture in Movie S1 of the Supplementary information. Under loading it usually suffers from catastrophic failure without noticeable ductility, which is fatal for structural applications. Actually, single-crystalline Ni_3Al have long been known to be ductile while their polycrystalline form was seen to be brittle. Many experiments have shown that the room-temperature ductility of polycrystalline Ni_3Al decreases dramatically when tested in moisture-containing environments, indicating a substantial environmental effect on ductility [8]. Therefore, reducing the propensity of brittle intergranular fracture is a key procedure towards ductilizing Ni_3Al. It is well-known that there is a traditional tradeoff dilemma between strength and ductility of materials. The covalent-like Ni–Al atomic bonding, on one hand, benefits the high intrinsic strength of Ni_3Al, which requires uniform breaking of the atomic bonds; on the other hand, it reduces the corresponding ductility. In principle, the pristine Ni_3Al has even higher theoretical strength than its related superalloys [4]. So that there seems to be a plenty of room for the potential applications of Ni_3Al for a mechanical purpose. However, there must be an effective strategy which can lead to a possible brittle–ductile

* Corresponding author. Tel.: +86 10 8254 3808.
** Corresponding author. Tel.: +86 10 8254 3958.
E-mail addresses: yjwang@imech.ac.cn (Y.-J. Wang), lhdai@lnm.imech.ac.cn (L.H. Dai).

http://dx.doi.org/10.1016/j.msea.2015.10.006
0921-5093/

transition of this material before the real applications.

Generally speaking, there are two pathways towards the ductilization of the brittle materials. The first choice is the chemical doping. It has been shown in experiments that the minor content of boron addition can dramatically increase the ductility of polycrystalline Ni_3Al [6]. The segregation of boron is beneficial for the grain-boundary cohesion and thus changes the fracture mode from intergranular to transgranular. As a result, the ductility is improved. While here we focus on another strategy, which is targeted at improving the intrinsic mechanical properties and modulating the fracture modes of the pristine Ni_3Al from its microstructure without involving doping effect.

Recently, size effect introduces significant advancement into the performance of mechanics of materials [9,10]. The strength of material is usually increased with decreasing grain size, or sample size, following a classical Hall–Petch relationship. In particular, the introduction of coherent twin boundaries (TBs) into sub-micron grains has greatly optimized strength without compromising too much ductility [11–16]. Especially, a very recent experiment indicates that deformation twinning could improve both strength and fracture toughness of high-entropy alloys [17]. All the new findings almost throw out the conventional idea that smaller is stronger, but more brittle, and less tougher in metallic crystals [9,18,17]. Molecular dynamics (MD) simulations show that TB could effectively block the motion of dislocations but allow its penetration partially [19]. This unique feature of dislocation-twin interaction excludes TB from other general high-angle grain boundaries in strengthening materials. Very recently, even the covalently bonded materials, e.g., diamond, and boron nitride, exhibit unprecedented hardness and stability via nanotwinning [20,21]. The present study is motivated by these amazing nanotwinned metallic and covalent materials. We wonder if a nanotwinned Ni_3Al can also show high strength and acceptable ductility simultaneously; as those have been achieved in both pure metallic- and covalently bonded nanotwinned materials. While the bonding nature in Ni_3Al is between metals and ceramics.

The main objective of this work is designing a strong and also ductile Ni_3Al nanostructure via a 'bottom-up' strategy. According to the experimental observations, deformation twinning is an important deformation mechanism of Ni-based superalloys at intermediate temperature and low strain rate conditions [5]. The deformation twins are found to initialize in the γ' precipitate of superalloys by nucleation of identical Shockley partials $a/6\{111\}\langle 112\rangle$, on consecutive $\{111\}$ planes. Therefore it seems to be possible in principle to prepare a real twinned Ni_3Al structure. Recently, bulk nanostructured Ni_3Al can be achieved via severe plastic deformation by high pressure torsion (HPT) [22–27]. In some cases, a large density of nanotwins are noticed by transmission electron microscopy in the nanocrystalline grains [25–27]. Moreover, a recent promising experiment has shown that ultrahigh strength can be achieved in twin-free Ni_3Al nanocubes [28]. It also shows possible homogeneous deformation with long elongation in the mentioned dislocation-free nanosized Ni_3Al cubes. All the above experimental phenomena motivate us to make a primary atomic-scale estimation on the intrinsic mechanical performance of the nanotwinned Ni_3Al in comparison with its twin-free counterpart.

The first-principles calculation with electronic details is the most robust tool to understand the ideal, or intrinsic mechanical properties of a perfect crystal accurately [29]. It predicts very reliable elastic constants [4], theoretical strength [29], some of the defect energetics [30–32]. However, there are usually size limitations in density functional theory (DFT) calculations which cannot deal with a real system containing large extrinsic defects, e.g., crack, dislocations, surface, and grain boundaries, etc., with typical size much larger than the available spatial scale of quantum mechanics. But the meaningful strength of a large-volume structural material with engineering relevance is usually governed by its fracture toughness instead of the ideal strength which is only associated with the uniform bond breaking strength [29,33]. Alternatively, classical MD with a reliable empirical interatomic potential could be an alternative method for understanding the microscopic deformation mechanisms, fracture modes, and the mechanical properties of nanostructures which are usually dominatingly governed by their extended defects [13,34–38]. The reliability of MD is strongly related to the choice of empirical potentials. There are also time-scale limitations in MD which lead to very high strain rates in deformation. Fortunately, hundreds of nanometers are sometimes large enough to mimic a metallic nanostructure, which can be handled effectively by MD. Depending on specific problems, MD can recognize important deformation mechanisms even at high strain rates [13,34–38]. In the case of Ni_3Al, atomistic simulations have

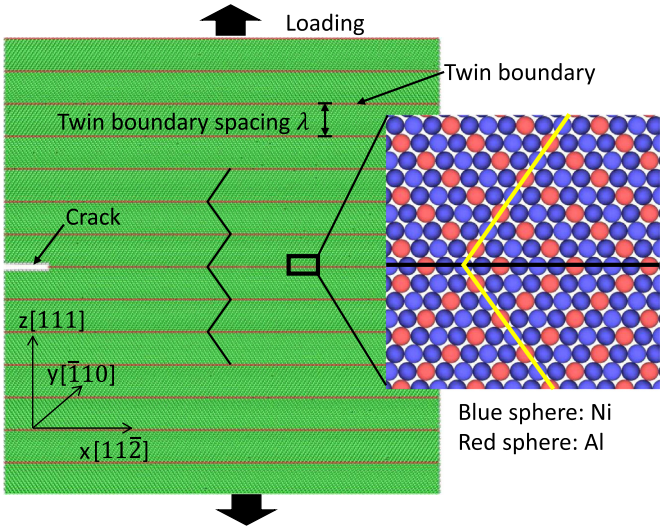

Fig. 1. An atomistic mode I crack model for modelling the fracture of nanotwinned Ni_3Al. Atomistically sharp $(111)[11\ \bar{2}]$ nanocrack is inserted into the middle of the nanotwinned sample on the left side. The twin boundary spacing is controlled from 0.62 nm to 9.90 nm. The magnified right inset shows the atomic arrangement of $L1_2$ real twin structure, with an exact mirror display of atoms sharing a common (111) plane. Long-range tensile loading along [111] direction facilitates the crack propagation. Atoms are colored by their CNA. Green: $L1_2$; red: HCP; white: others. (For interpretation of the references to color in this figure caption, the reader is referred to the web version of this paper.)

already shown novel deformation mechanisms when the sample size is reduced to the form of nanocubes [39], or nanopillars [40]. Here we focus on the fracture of Ni_3Al nanotwinned structures with a reliable empirical potential [41].

In this work, we adopt an atomic-level crack model to highlight the superior mechanical performances of Ni_3Al nanotwinned structure. We find a surprising 'smaller is stronger, but still tougher' trend, which is in sharp contrast with the conventional idea that high strength deserves poor ductility and low toughness. A novel quasi-brittle fracture mechanism of pristine Ni_3Al is uncovered with nucleation of twinning dislocations from crack tip. We also notice an interesting transition of fracture mechanism in nanotwinned Ni_3Al from dislocation nucleation to shear localization due to competition between twin spacing and the critical size of nucleated dislocation. Possible energetics analysis is provided to understand the correlation between the macroscopic mechanical behaviors and the atomic-level observations of cracking mechanisms.

2. Computational details

2.1. Model setup

Atomic-level crack model has been widely adopted to study the intrinsic mechanical properties of materials [42,37,43,33,44,45]. Here we use a similar strategy. Fig. 1 shows the geometry of an atomic-scale mode I crack model of nanotwinned Ni_3Al. The atoms in twin and matrix of $L1_2$ Ni_3Al share a common {111} mirror plane. The detailed atomic arrangement near the twin boundary is magnified and shown as the inset of Fig. 1. All Ni and Al atoms follow an exact mirror display, as labeled by the zigzag black line in the main figure, and the yellow lines in the inset, respectively. An atomistically sharp nanocrack with a length of 5 nm and a height of 1.6 nm is created on the low surface energy close-packed plane (which is the {111} twin plane) of Ni_3Al, with the crack front parallel to the ⟨110⟩ direction. In this case, the propagation direction of the crack is ⟨112⟩. The dimensions of these 3-dimensional crack samples are about 50 nm × 5 nm × 50 nm (~880,000 atoms), depending on the choices of twin boundary spacing λ. The convergence of deformation mechanisms in the crack models has been checked against larger models. In the present modelings, we vary λ from 0.62 nm (the possible smallest twin size with a complete ABC stacking sequence of the $L1_2$ structure along ⟨111⟩ direction) to as large as 9.9 nm, in order to investigate the size effect on their fracture behaviors. A twin-free pre-cracked model is also created in comparison with these nanotwinned samples.

2.2. Molecular dynamics

The present atomistic simulations are performed by the Large-scale Atomic/Molecular Massively Parallel Simulator (LAMMPS) [46]. The force field is described by an embedded-atom method (EAM) potential for Ni–Al system [41]. This potential is built by fitting to both experimental and first-principles data. It can predict very accurate lattice and mechanical properties, energetics of point defects and planer faults, which are of vital importance to study the cracking behavior of Ni_3Al [41]. It has been widely used to investigate the deformation mechanisms of Ni_3Al nanostructures, which include both nanowire and nanocube [40,39]. To drive the propagation of mode I crack, long-range uniaxial tensile loading on ⟨111⟩ direction (perpendicular to the crack surface and twin plane) is applied with a constant strain rate of $10^8\ s^{-1}$. The MD time step is 2 fs. Note that very high strain rate is applied to the crack model within the short MD time window. High strain rate drives the displacive deformation modes (dislocation nucleation and motion) to occur at short time scale since the high stress level significantly reduces the activation free energy barrier. However, the diffusive mechanisms are not very sensitive to the external stress and cannot be included in the present MD modellings at low temperature. Therefore, we may miss the long time-scale diffusion mechanisms which is required to transform a pseudo-twin to a real twin structure in Ni_3Al [5]. In order to obtain the intrinsic toughness of the pre-cracked nanotwinned samples, the simulations are carried out at 1 K with a *NPT* ensemble, to rule out the thermal noises [34]. Here *N*, *P*, and *T* denote the number of atoms, pressure, and temperature, respectively. Nosé–Hoover thermostat is utilized to keep constant temperature [47,48]. Parrinello–Rahman technique is adopted to control the stress tensor [49]. Free surface is generated on *x*: [11$\bar{2}$] direction to avoid the image effect of crack propagation, while periodic boundary conditions (PBC) are applied on the *y*: [$\bar{1}$10] and *z*: [111] directions. During the uniaxial loading, the transverse directions are free to relax and are kept a stress-free condition. The atomic-level stress tensor is calculated according to Virial theorem. The defects of $L1_2$ Ni_3Al are mostly recognized by common neighbor analysis (CNA), and visualized by the softwares OVITO [50] and ATOMEYE [51].

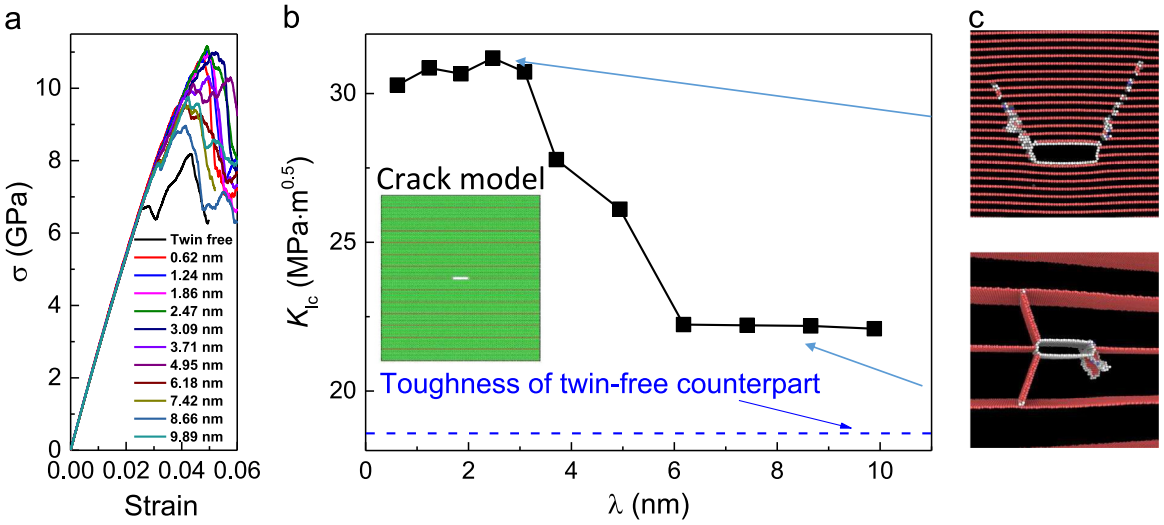

Fig. 2. Fracture toughness of the nanotwinned Ni_3Al. (a) Stress–strain curves of the pre-cracked samples with varied twin size λ. (b) Fracture toughness increases with decreasing λ, indicating a 'smaller is tougher' trend. (c) MD snapshots demonstrate the cracking mechanisms of nanotwinned Ni_3Al. Upper panel: shear localization; and lower panel: dislocation nucleation initiates from the crack tip; depending on the twin size. Only imperfect atoms are shown according to CNA.

3. Results and discussion

3.1. Smaller is tougher

According to the classic Griffith criterion [52], brittle fracture happens if the release of the strain energy exceeds the surface energy generated by the two new crack surfaces for an infinitesimal crack propagation. The fracture stress is described in this framework as

$$\sigma_c = \sqrt{\frac{2E\gamma_s}{\pi a_0}}. \quad (1)$$

Here E is Young's modulus, γ_s the surface energy, and a_0 the half length of the crack. The fracture stress σ_c is actually the critical stress of the onset of crack propagation, or the stress level required to generate the first plastic event, such as dislocation emission in the present case. Note that surface effect could lead to big uncertainty in the estimation of fracture stress and toughness, the crack is moved into the center of the models which are described by PBC on each direction, see the geometry in the inset of Fig. 2(b). For the $\{111\}\langle 112\rangle$ pre-cracked pristine Ni_3Al, E=283 GPa and $\gamma_s = 1.48\ J/m^2$ can be estimated based on the present EAM potential. For a first approximation, the fracture stress of Ni_3Al can be predicted as $\sigma_c = 10.3$ GPa based on Eq. (1), in the case of $a_0 = 2.5$ nm, as which is adopted in our model setup. This estimated magnitude is of a correct order of direct MD prediction, which is about 8.2 GPa as shown in Fig. 2(a). It means that the Griffith theory is approximately applicable even down to the atomic level, at least in the present crack model of Ni_3Al.

The fracture toughness, according to the present atomistic model, can be estimated as

$$K_{Ic} = \sigma_c\sqrt{\pi a_0}, \quad (2)$$

where K_{Ic} is the critical stress intensity factor of mode I crack. Fig. 2 shows the twin size effect on the calculated fracture toughness of the nanotwinned Ni_3Al samples. The results of pristine Ni_3Al is also listed for comparison.

Fig. 2 (a) shows the stress–strain curves of the pre-cracked nanotwinned Ni_3Al samples with $\lambda \sim 0.62$–9.89 nm, along with the result for their twin-free counterpart. The critical stresses of these pre-cracked samples are around 10 GPa, which is substantially lower than the ideal tensile strength of Ni_3Al on $\langle 111\rangle$ direction. The latter is ~27 GPa [40], which is estimated by the present EAM potential [41]. Since the ideal strength is in principle governed by the uniform breaking of atomic bonds, whereas the fracture stress is relevant to a heterogenous plastic event near the crack tip, therefore a big gap exists between the two mechanical parameters. Note that there are more than 10 times difference in the density of twin boundaries in our models, which allows us to obtain a clear insight into the size effect of cracking in nanotwinned structures. It is interesting to find that the peak stress (or critical stress) of all the nanotwinned samples are larger than their twin-free counterpart, which is shown as the black curve in Fig. 2(a). It implies that nanotwinning could be an effective pathway towards toughening Ni_3Al. As shown in Fig. 2(b), the estimated fracture toughness of all the twinned sample are higher than that of the twin-free one, which is approximately 18.7 MPa $m^{0.5}$. The latter is in reasonable agreement with the experimental data 20.0 ± 2.5 MPa $m^{0.5}$ [53]. This agreement validates our methodology to estimate the fracture toughness of Ni_3Al from the atomic-level. More interestingly, there exists an obvious 'smaller is tougher' trend in these nanotwinned samples. The fracture toughness increases with decreasing twin size λ. It reaches a maximum in fracture toughness of about 31.2 MPa $m^{0.5}$ when $\lambda < 3$ nm. This value is approximately 70% higher than that of twin-free Ni_3Al. The result is surprising since there is usually a tradeoff dilemma between strength and toughness [18,16]. Once

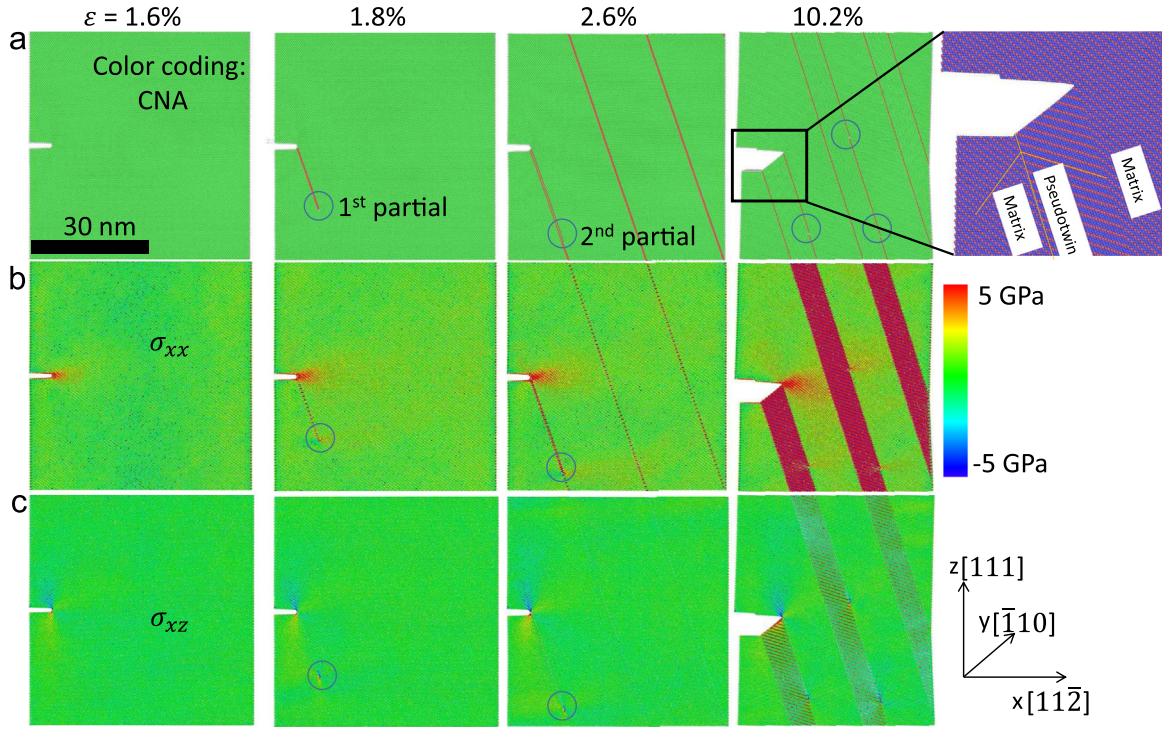

Fig. 3. Deformation twinning induced quasi-brittle fracture mode of twin-free Ni_3Al. (a) Atomic structure, (b) atomic stress σ_{xx}, and (c) σ_{xz} distribution at different magnitudes of strains. Layer-by-layer $a/6\{111\}\langle 112\rangle$ Shockley partial dislocation nucleation from crack tip leads to the nanotwinning mechanism of crack propagation. The crack tip propagates in a quasi-brittle manner with emitting partial dislocations from crack front, leaving free surfaces behind. The most right inset of (a) shows the atomic pseudotwin structure. Atoms in (a) are colored by CNA in the main plot. The deformation mechanisms are further detailed in Movie S2 of the Supplementary Information. (For interpretation of the references to color in this figure caption, the reader is referred to the web version of this paper.)

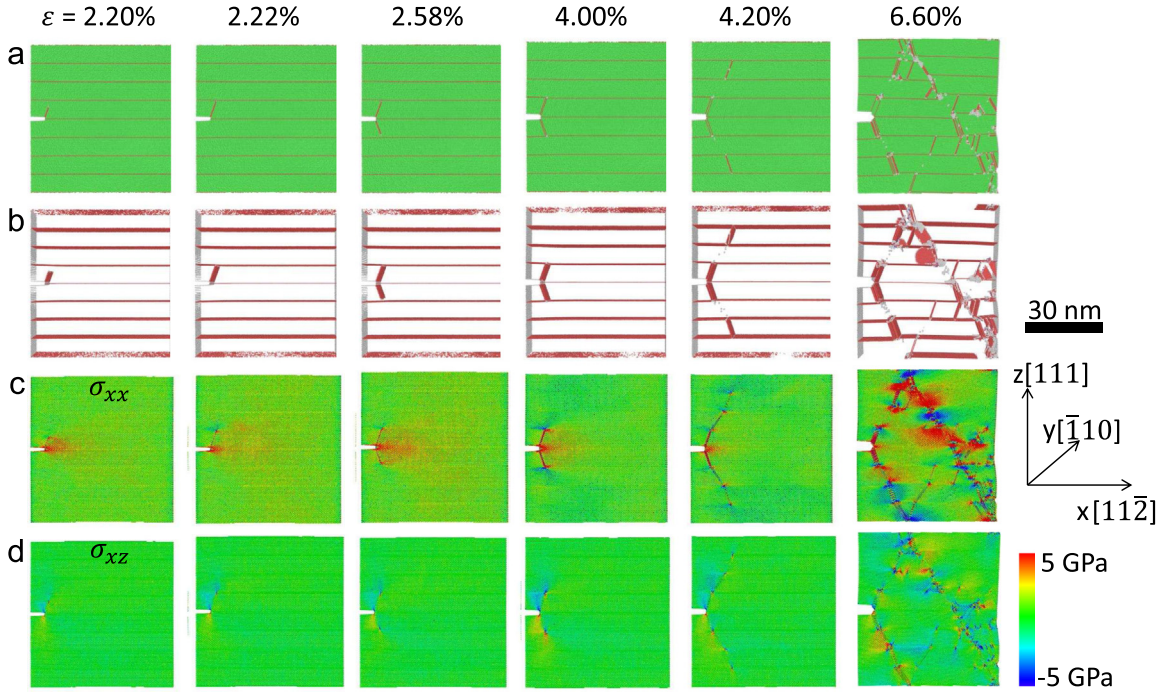

Fig. 4. Dislocation nucleation governed ductile fracture mode of λ=6.2 nm nanotwinned Ni_3Al. (a) Atomic structure, (b) defective structure, (c) σ_{xx}, and (d) σ_{xz} distribution at different magnitudes of strains. Two partial dislocations first nucleate from crack tip, and then their propagations are blocked by the pre-existing twin boundaries. Two smallest twin forms at ε=4.00%, and stress is concentrated at the intersection of twin boundaries and dislocations. With increasing stress concentration, dislocations penetrate the twin boundaries. Crack blunting occurs once it is surrounded by dislocation avalanches after ε=6.60%. Atoms in (a) and (b) are colored by CNA, while perfect $L1_2$ atoms are removed for clarity in (b). Details are further provided in Movie S3. (For interpretation of the references to color in this figure caption, the reader is referred to the web version of this paper.)

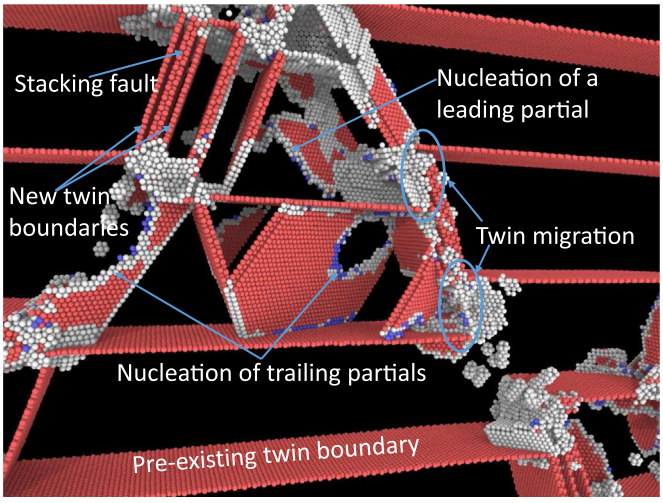

Fig. 5. Closeup of the deformation pattern of λ=6.2 nm nanotwinned pre-cracked Ni_3Al. Multiple plastic mechanisms are observed, i.e., leading and trailing partial dislocation nucleations, stacking fault, and twin migration. Atoms are colored by CNA; perfect $L1_2$ atoms have been removed for clarity. (For interpretation of the references to color in this figure caption, the reader is referred to the web version of this paper.)

the material becomes stronger with grain or sample refinement, it often losses toughness. However, the present strategy of nanotwinning sheds light on increasing toughness and strength of covalent-like bonded materials at the same time. Furthermore, there seems to be a sharp transition in toughness when λ is smaller than 6 nm. The MD snapshots in Fig. 2(c) show the underlying mechanism shift behind the transition. When λ > 6 nm, dislocation nucleation from crack tip dominates the cracking (lower panel), while strong shear offset is noticed in the vicinity of the crack tip if λ < 3 nm (upper panel). This interesting transition of cracking mechanisms in nanotwinned Ni_3Al will be detailed and rationalized in this work.

3.2. Fracture mechanisms

3.2.1. Fracture mechanism of twin-free Ni_3Al

It is well-known that Ni_3Al is very brittle in polycrystalline form due to the intergranular fracture mode [6,1]; see an example of Σ7 cleavage demonstrated by Movie S1 in the Supplementary information. In this work we focus on fracture of the single-crystalline, and nanotwinned Ni_3Al. We first clarify the fracture mode of the twin-free pristine Ni_3Al. The cracking mechanism is shown in Fig. 3 at very high temporal resolution in order to catch important plastic events. The atomic structures, and their instantaneous stress tensor distribution of σ_{xx} and σ_{xz} are shown in Fig. 3(a), (b), and (c), respectively, at different levels of tensile strain ε. ε=1.6% is the case just before the first plastic event appears. We cannot notice any defective structures except the pre-existing crack, but significant stress concentration of both σ_{xx} and σ_{xz} is noticed at the crack tip. Such high stress concentration leads to the first Shockley partial dislocation ($a/6\langle 112\rangle$) nucleating from the crack tip, as labeled by a circle at ε=1.8%. The nucleated leading partial travels across the whole sample before it reaches at the opposite free surface of the crack model. At ε=2.6%, the second leading partial is nucleated at the adjacent (111) plane, which forms a smallest apparent deformation twin with thickness of just two atomic layers. The same process repeats again and again, eventually the apparent deformation twin grows larger and larger via this twin migration mechanism. In this way, crack propagates sharply on the [11 $\bar{2}$] direction, leaving two free {111} surface behind; see details in Fig. S1 of the Supplementary information. This manner of crack propagation is different from the conventional cleavage mechanism of brittle fracture, but crack still

propagates very sharply which is maybe termed as a 'quasi-brittle' manner. The scenario of quasi-brittle fracture via releasing deformation twinning may be a new cracking mechanism besides the intergranular fracture for such covalent-like bonded metallic materials. Actually, it is frequent to notice deformation twinning in the γ' phase of Ni-based superalloys [5]. The present finding may suggest deformation twinning as a novel plastic deformation and fracture mechanism of Ni_3Al.

The enlarged atomic structure of apparent deformation twin at $\varepsilon = 10.2\%$ is shown as the most right panel of Fig. 3(a). It denotes an actual pseudo-twin structure of Ni_3Al. Although the atoms form a mirror display on the two sides of (111) twin boundary plane, Ni and Al atoms in twin are not on the exact mirrored positions of the matrix. Such deformation pseudo-twinning mechanism is also noticed in NiTi alloy with B2 structure [35]. This findings of pseudo-twinning may come from the time-scale limitation of MD. It actually takes further shuffling mechanisms after shear to form a real twin in NiTi [54,55]. The pseudo-twin in Ni_3Al is not stable since Al atoms lie in the unfavorable nearest neighboring positions. This is illustrated by the extremely high stress concentration in the twinned region; as displayed in Fig. 3(b) and (c). Note that this pseudo-twin will finally transform to a real twin by some possible diffusive mechanisms in Ni_3Al [5]. The process has been clarified by first-principles calculations [5]. However, the diffusive process cannot be observed in the short time window of classic MD. While in experiments, disordered nanotwins are observed after HPT [25–27]. There is no long-range ordered structure in the disordered twin. The formation of such disordered twin requires disordering before twinning. In summary, the twin-free Ni_3Al fractures in a novel quasi-brittle manner with sharp crack propagation by emitting twinning partials on the consecutive {111} planes. As we know, twin boundaries are effective blocks for the motion of dislocations. So that it seems possible to suppress this special manner of crack propagation by inserting high density of twin boundaries into pristine Ni_3Al, which possibly gives rise to a brittle–ductile transition.

3.2.2. *Fracture mechanism of wide nanotwinned Ni_3Al*

Fig. 4 shows the fracture mode of a nanotwinned Ni_3Al with $\lambda = 6.2$ nm. Dislocation nucleation replaces deformation twinning as a ductile fracture mechanism due to an interaction between nucleated dislocations and pre-existing twin boundaries. As

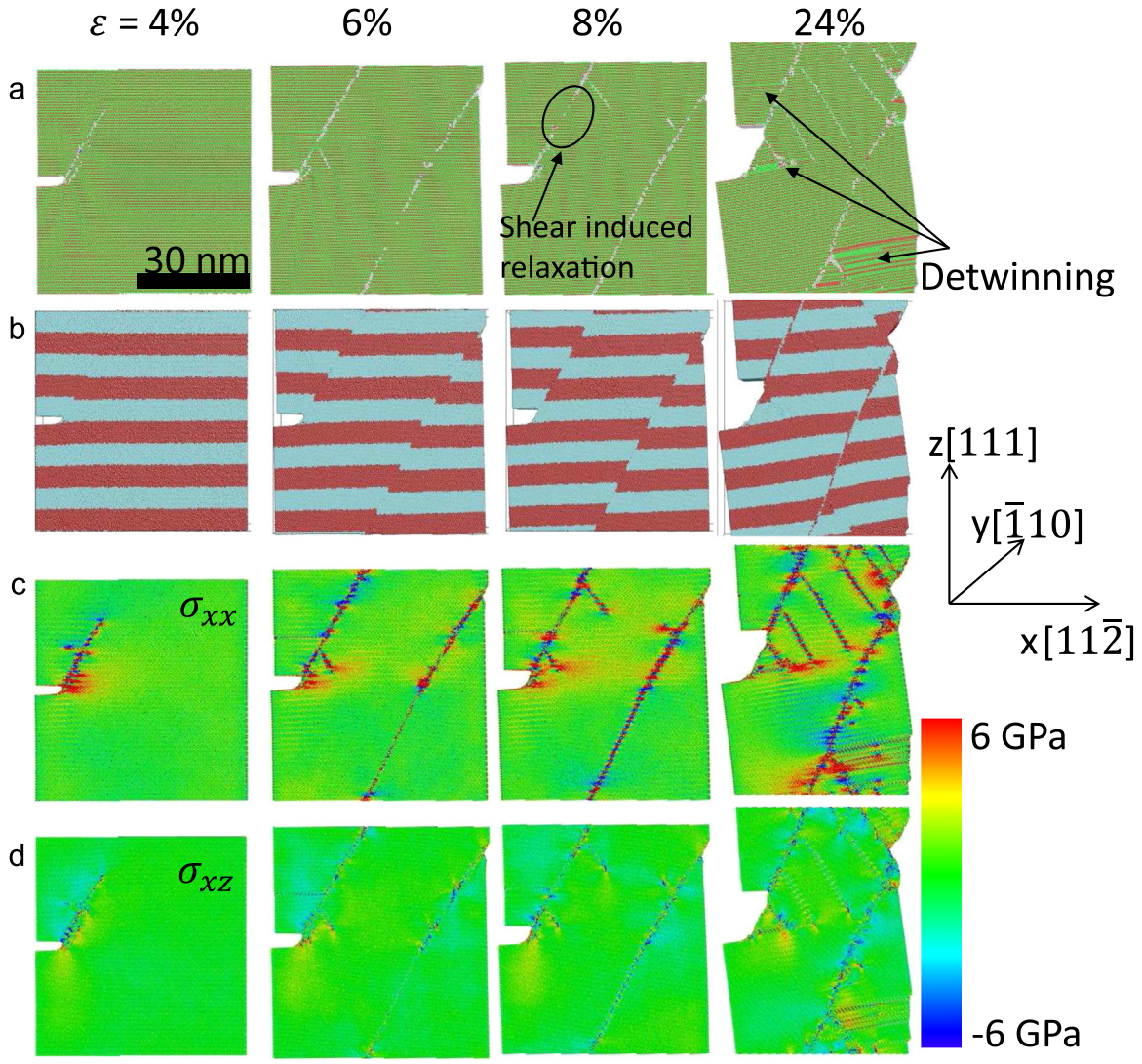

Fig. 6. Shear localization dominates fracture of $\lambda = 0.62$ nm nanotwinned Ni_3Al. (a) CNA color coding, (b) tiling blocks color coding, (c) σ_{xx}, and (d) σ_{xz} distribution at different levels of strains. Shear localization is revealed as the dominant fracture mode in the nanotwinned Ni_3Al with extremely high twin density. During deformation process, occasionally, the shear offset can heal itself by continuing shear displacement when two twin boundaries meet each other, as shown by the black ellipse at $\varepsilon = 8\%$. Detwinning is also observes at $\varepsilon = 24\%$. Details are further provided in Movie S4. (For interpretation of the references to color in this figure caption, the reader is referred to the web version of this paper.)

shown in Fig. 4, the first partial nucleates from crack tip a bit earlier than ε=2.20%. This partial should travel freely without obstacles in the twin-free sample. However, the pre-existing twin boundaries stop the propagation of the traveling dislocations at ε=2.22%. Consequently, stress is concentrated in the intersection of twin boundary and dislocation front, as illustrated by the stress distributions in Fig. 4(c) and (d). Then, the second partial emits on the opposition side of the crack, and it is again blocked by the neighboring twin boundary. The process is demonstrated by the plots at ε=2.58%, and ε=4.00%, respectively. In this way, the pre-existing twin boundaries suppress the formation of deformation twinning, which has been shown as a quasi-brittle cracking mechanism of twin-free Ni_3Al.

It is also interesting to notice that dislocations can penetrate the twin boundaries with the help of high stress concentration on the intersection of dislocation and twin boundary, which is shown at ε=4.20% in Fig. 4. The scenario is that first two partials nucleate from the crack tip, and then are blocked by the first nearest twin boundaries. With the critical role of even more stress concentration in the intersection of dislocations and twin boundaries, the stopped leading partial dislocations penetrate the first nearest twin boundary and are followed by trail partial dislocation. After the full dislocation slip, there leaves no stacking fault between the first and second nearest twin boundaries. The trailing dislocation can be observed as the white line in the stacking fault between the second and third nearest twin boundaries, as shown in Fig. 4(b) at strain of ε=4.20%. So the first several dislocations nucleated from the crack tip are not random in nature but triggered by the stress concentration. While after the dislocation avalanches, the dislocation nucleation is sort of stochastic behavior within the stress

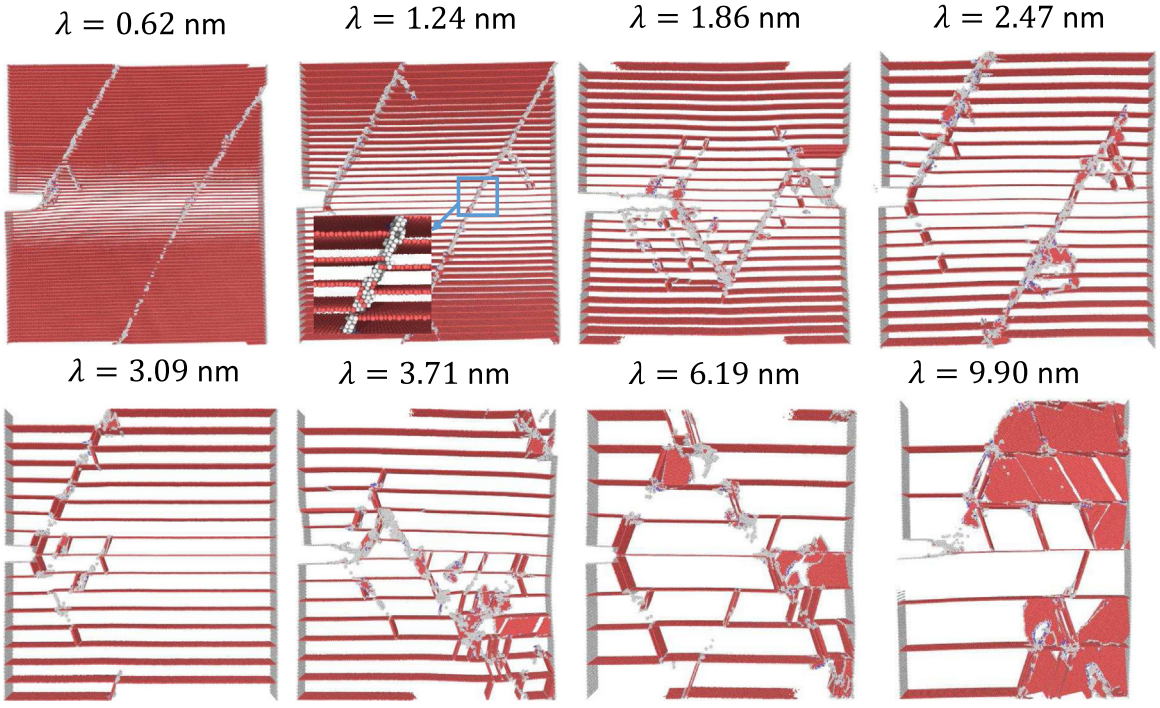

Fig. 7. Size-dependent transition of fracture mode in nanotwinned Ni_3Al. Dislocation nucleation is replaced by shear localization as the dominating cracking mechanism at a critical twin size of $\lambda \sim$ 2–3 nm. The configurations are shown at a strain value of ε=6 %. Atoms are colored by CNA and the perfect $L1_2$ atoms have been removed for clarity. (For interpretation of the references to color in this figure caption, the reader is referred to the web version of this paper.)

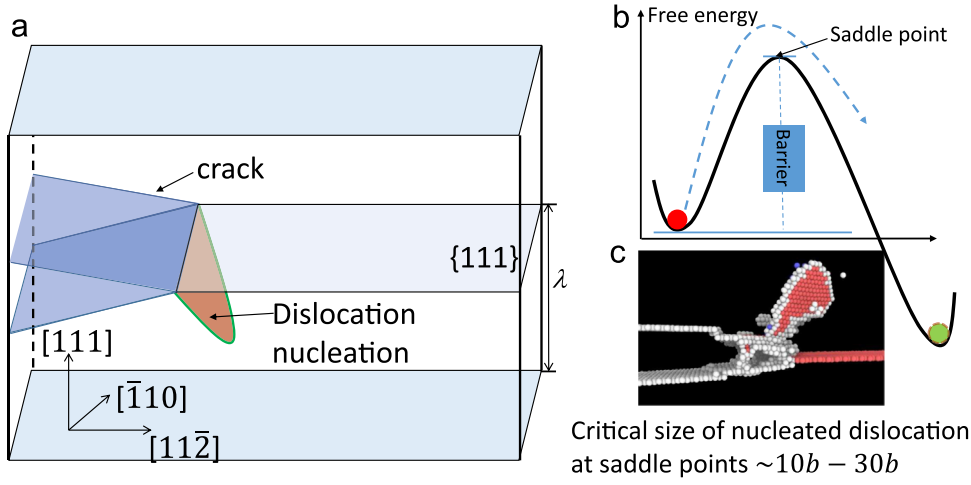

Fig. 8. Schematic demonstration of the interplay between dislocation nucleation size and twin spacing. (a) Geometry of a dislocation nucleation from crack tip of the nanotwinned sample. (b) Free energy landscape of a dislocation nucleation process. (c) A MD snapshot showing dislocation nucleation from crack tip.

concentration region. The phenomenon is in good agreement with a previous atomistic reactive pathway sampling of dislocation-twin interaction in nanotwinned fcc metal [19]. With strain increases, dislocations avalanche in the vicinity of crack tip. The above scenario is the crack blunting mechanism of the relatively wider nanotwinned Ni_3Al. Compared with both brittle fracture of grain boundary (Movie S1), and quasi-brittle fracture of twin-free Ni_3Al (Movie S2), the present strategy of nanotwinning gives rise to a promising brittle–ductile transition, which is targeted to solve the long-standing bottleneck of Ni_3Al as a structural material.

A closeup of atomic structure in Fig. 5 implies more plastic deformation mechanisms in the vicinity of crack. The mechanisms include leading and trailing dislocations nucleation, formation of stacking fault, nucleation of new twin, as well as the twin migration due to the dislocation emission from dislocation-twin intersection. All the above-mentioned plastic mechanisms would benefit the ductility of nanotwinned Ni_3Al. Note that the initial position of the pre-existing crack has minor effect on the dislocation behaviors of cracking of nanotwinned Ni_3Al. In order to clarify this point, we also simulate a sample with initial crack setup in between two twin boundaries. The scenario of crack tip dislocation nucleation and propagation as well as interaction with twin boundaries keeps unchanged.

3.2.3. *Fracture mechanism of narrow nanotwinned Ni_3Al*

The toughness scaling in Fig. 2 indicates a transition of fracture modes which are induced by twin size reduction. Here we show and clarify how crack propagates in the very narrow-twin-sized Ni_3Al sample. Fig. 6 shows an example of extremely narrow twinned sample with λ=0.62 nm. It is clear to see that strong shear localization happens on the {111} plane with the largest resolved shear stress. The tiling block color coding method shown in Fig. 6(b) can track the instantaneous position of atoms by remembering their original color [51]. Obvious shear localization in the vicinity of crack tip can be visualized by the trick. The shear localization initializes from the crack tip, and then it propagates across the whole sample regardless of the obstacles served by the pre-existing twin boundaries. This phenomenon is actually a rigid shear mechanism of the neighboring {111} planes, which is equal to homogeneous dislocation nucleation. It requires a critical resolved shear stress (CRSS) comparable to the ideal strength of a material (Σ3 twin boundary is the most stable grain boundary). This is the reason why nanotwinned Ni_3Al shows very high toughness once the twin size is smaller than a critical value of about 3 nm, since the fracture stress is approaching to the ideal strength (Fig. 2).

It is also worthy to notice that the shear localization can sometimes induce structural recovery with the continuous shear offsetting, as labeled by the ellipse in the case of ε=8%. At larger strain of 24%, detwinning happens since there begins to exist shear stress component on the pre-existing twin boundaries. Stress distribution indicates reorientation of crack propagation (ε=8%, 24%), with a significant role of stress concentration played at the intersections of twin boundaries and the shear offsets. We note that this shear-banding-like behavior may be harmful to the ductility of Ni_3Al. Shear localization may facilitate the nucleation of crack which finally leads to a brittle fracture phenomenon in the extremely narrow nanotwinned alloy. This is not anticipated for structural applications. As a result, the twin size cannot be too small in order to design a simultaneously ductile and tough nanotwinned Ni_3Al.

3.3. *Twin-size-dependent transition of mechanisms*

In this section, we clarify why the variation in twin size can lead to a transition of fracture mechanism in nanotwinned Ni_3Al. Fig. 7 lists the deformation modes of pre-cracked nanotwinned samples with λ between 9.90 nm and 0.62 nm. There is a clear trend from dislocation nucleation dominating cracking mechanism to shear localization with decreasing λ. The transition occurs at $\lambda \sim$ 3–6 nm, which coincides with the abrupt increase in toughness as shown in Fig. 2. This is the microscopic mechanism underlying the discovered 'smaller is tougher' trend. For comparison, similar mechanism transition has been detected by MD simulations in copper nanopillars [34]. The inset of λ=1.24 nm sample shows the atomic details of rigid shear of the nanotwinned sample on {111} slip planes. The rigid shear should be driven by extremely high stress that is almost identical to break a perfect crystal since the coherent twin boundary has very high cohesive strength.

Fig. 8 demonstrates why the transition of fracture mechanism happens from a physical point of view. The geometry of a crack tip dislocation nucleation is shown in Fig. 8(a), while Fig. 8(b) is the corresponding free energy landscape. Fig. 8(c) denotes a real case of crack dislocation nucleation from MD simulations. Dislocation nucleation process completes once the applied stress can facilitate to overcome the free energy barrier. The saddle point structure of the nucleated dislocation requires a critical space. Previous atomic reactive pathway sampling form Zhu et al. confirms that the critical size d_c of dislocation saddle point structure is ~10b–30b [56], here b is the magnitude of Burgers vector of the nucleated dis-

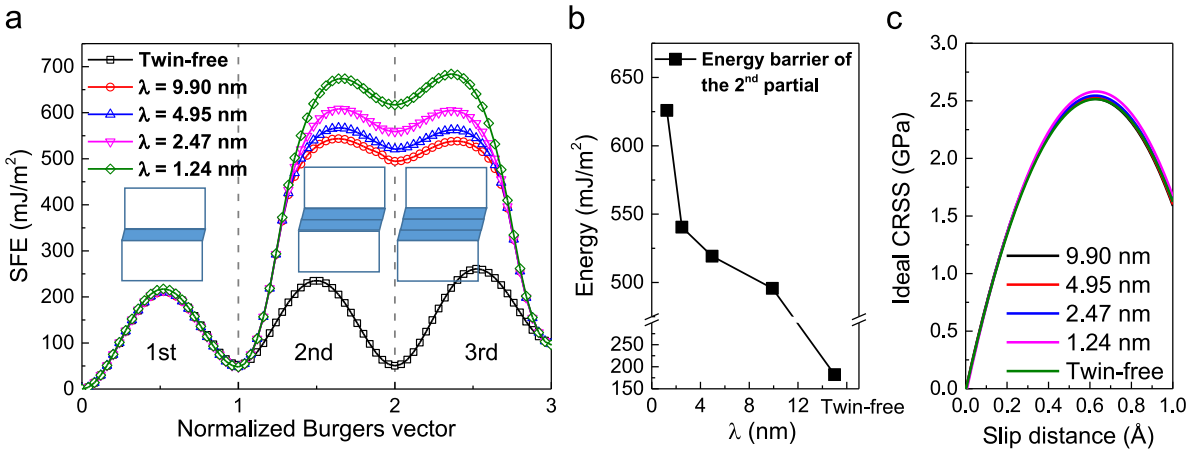

Fig. 9. Size effect on the twinnability of the nanotwinned Ni_3Al. (a) Energy profile of the deformation twinning pathway for twin-free and nanotwinned Ni_3Al with different twin sizes. (b) Energy barrier of the second partial dislocation nucleation as a function of twin size. (c) Ideal CRSS of the nanotwinned Ni_3Al with different twin sizes.

location. In the case of Ni_3Al, $b=1.52$ Å is for the $a/6\{111\}\langle 112\rangle$ Shockley partials. So that the critical size of dislocation nucleation should be of the order of about 1.5 – 4.5 nm. While our MD predicts the critical size is approximately 3 nm, as shown in Fig. 7, which is on a correct order of the theoretical estimation. Thereafter the cracking mechanism actually depends on the competition between twin size λ and the critical size d_c of dislocation loop at saddle point. If $\lambda > d_c$, heterogenous dislocation nucleation is allowed from a crack tip; otherwise, rigid shear (or homogeneous dislocation nucleation) governs the fracture mechanism of the nanotwinned Ni_3Al.

3.4. Energetics analysis

Our MD modelings predict that twin boundaries could block the motion of twinning dislocations. The brittle grain boundary fracture mode and the quasi-brittle fracture mode of twin-free single-crystalline Ni_3Al can be significantly suppressed once the material is nanotwinned. Instead, heterogenous or homogenous dislocation nucleation may lead to some possibility of cracking blunting. Here we perform energetics analysis to furthermore understand the size effect on the twinnability of a pre-nanotwinned Ni_3Al. The results are summarized in Fig. 9. The inset in Fig. 9(a) denotes schematically the process of successive stacking fault formation on consecutive adjacent {111} planes due to the partial dislocation nucleation. The rigid shear is controlled to take place in the middle of a twin/matrix (far from twin boundary to reduce possible interaction).

The twin-size-dependent stacking fault energy (SFE) profiles are plotted versus normalized Burgers vector, as shown in the main plot of Fig. 9(a). To form a deformation twin, at least a second stacking fault should be generated on the neighboring plane of the first one with a shift of one Burgers vector. Therefore, the second SFE is a critical parameter to determine whether a deformation twin can form or not. It is noticed that all the nanotwinned samples have much larger SFE after the first partial compared with that of their twin-free counterpart. Fig. 9(b) shows that the energy barrier of the second partial dramatically increases with decreasing twin size. This is the physical origin why the deformation twinning is very difficult in the pre-nanotwinned sample in contrast with the twin-free one. As a result, nanotwinning could be an effective way to drive a possible brittle–ductile transition in Ni_3Al since the quasi-brittle fracture mode which requires deformation twinning can be greatly suppressed.

We further define an ideal CRSS(i-CRSS) [29]

$$\tau_{i-\mathrm{CRSS}}(\vec{x}) = d\gamma(\vec{x})/d\vec{x}, \tag{3}$$

as the maximum stress required to drive the first rigid shear (homogenous dislocation nucleation) between two neighboring {111} planes, as that illustrated in the inset of Fig. 9(a). Here $\vec{x}$ is the relative displacement vector of the two neighboring slip planes. $\gamma(\vec{x})$ is the corresponding SFE with slip vector $\vec{x}$. Fig. 9 (c) displays the i-CRSS of the nanotwinned Ni_3Al with different twin sizes in comparison with twin-free one. There is almost no difference in i-CRSS of these nanotwinned and the twin-free samples. It is the reason why the fracture toughness (or the fracture stress) of the nanotwinned Ni_3Al reaches a plateau when the twin size is smaller than 3.0 nm, as shown in Fig. 2(b), where shear localization becomes the dominating plastic mechanism. In this regime, fracture stress is almost identical to the i-CRSS of the perfect Ni_3Al.

3.5. Smaller is stronger

Finally, we check the size effect on the intrinsic strength of the nanotwinned Ni_3Al single crystal. Columnar-shaped Ni_3Al nanopillar with different inserted densities of twin boundaries is adopted to represent a single crystal. The diameter of pillars is 20 nm, which include about 2,730,000 atoms. The geometry of the pillars is shown in Fig. 10(a). In order to obtain the strength, uniaxial tension is applied on the [111] direction with a constant strain rate of $10^8\ s^{-1}$ at 300 K. The peak stress which appears in the stress–strain curve is defined as the strength of these nanotwinned single crystals. The calculated strength and failure strain are plotted as a function of twin size in Fig. 10(b). It is interesting to find that strength and critical strain could be improved substantially by decreasing twin size. Such a 'smaller is stronger' trend discovered in Ni_3Al is exciting since we have already shown a 'smaller is tougher' trend in the nanotwinned samples. Therefore we can probably achieve high strength and toughness simultaneously in the nanotwinned Ni_3Al, while in most cases, toughness is sacrificed once strength is increased by reducing grain or sample size. In particular, the strength of the nanotwinned Ni_3Al reaches about 17.0 GPa when twin is reduced to its smallest size, i.e.,

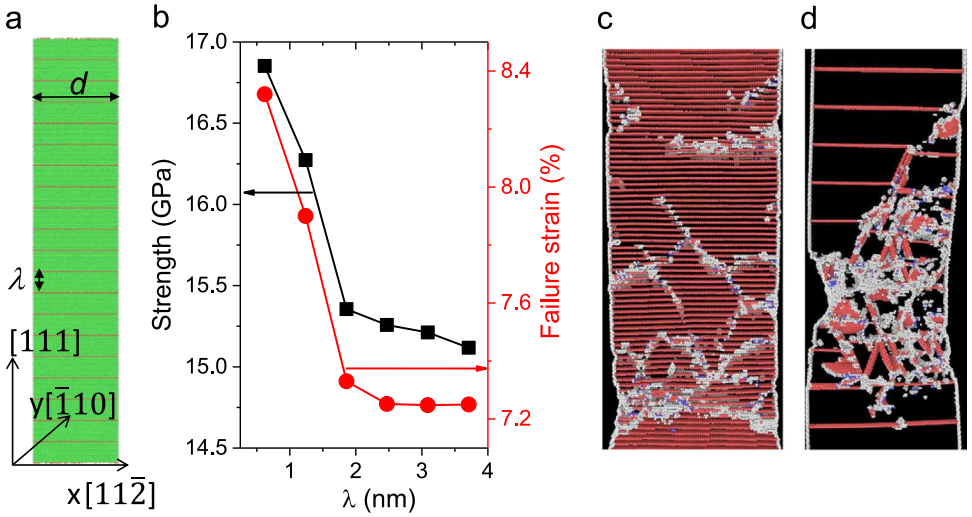

Fig. 10. 'Small is stronger' trend in the nanotwinned Ni_3Al single-crystal. (a) Geometry of the nanotwinned Ni_3Al single-crystalline nanopillar with diameter of 20 nm. (b) Strength and failure strain as a function of twin size. (c) Shear localization uncovered in the narrow twinned sample, with $\lambda=0.62$ nm at $\varepsilon=10\%$. (d) Dislocation nucleation recognized in the wider twinned sample, with $\lambda=4.95$ nm at $\varepsilon=7\%$. Only defective atoms are shown in (c) and (d) which are distinguished by their CNA number.

$\lambda = 0.62$ nm. Such a high strength is almost comparable to the ideal tensile strength ~25.0 GPa of Ni_3Al on the [111] direction, according to a first-principles estimation [4]. Note that the ideal strength is the upper limit of stress that a material can sustain before the uniform bonding breaking, it should be much higher than the actual strength of a real material in which plastic deformation involving pre-existing defects is allowed, such as heterogeneous dislocation nucleation [29].

Moveover, we also find an abrupt increase of strength when the twin size is smaller than ~2.0 nm. Fig. 10(c) and (d) confirms that there exists a transition of deformation mechanism from dislocation nucleation to shear localization with decreasing λ below a critical value. The transition is similar to the transition in fracture mode of the pre-cracked nanotwinned Ni_3Al. Combined with a similar transition discovered in the nanotwinned copper nanopillar [34], it is postulated that size-induced transition of heterogenous (nucleation from defects, such as surface, grain boundary, and crack tip) and homogenous (rigid shear, extremely localized deformation) dislocation nucleation is general in the nanotwinned metals. Finally, we note that the surface stress plays an important role in determining the failure strength and strain of these nanotwinned nanopillars. In our previous study, the surface stress can drive the deformation mechanism from dislocation nucleation to phase transformation with decreasing pillar diameter [40].

4. Summary

Ni_3Al exhibits superior mechanical properties at elevated temperature due to its long-range order $L1_2$ superlattice. It is frequently used as a strengthening phase (γ') in the Ni-based superalloys. Ni_3Al itself has even higher theoretical strength than that of the Ni solid solution (γ phase), which provides a plenty of room for the utility of Ni_3Al as creep-resistance materials in high temperature environment. However, the pristine Ni_3Al is very brittle due to the notorious intergranular fracture and the covalent-like atomic bonding. The brittle nature is a long-standing unsolved issue of Ni_3Al, which hinders its vast applications as structural materials. Generally, reducing grain size or sample size down to nanoscale leads to high strength, but this strategy usually compromises ductility and toughness.

Here we use atomistic simulations to highlight the critical role of nanotwinning in the mechanical properties of Ni_3Al, which is based on an atomic-scale cracking model. The present atomistic model can predict reliable toughness scale of pristine Ni_3Al which is verified by the experimental data. It is quite surprising to find a 'smaller is stronger', and meanwhile 'smaller is tougher' phenomenon in nanotwinned Ni_3Al. Its strength and toughness are both improved with increasing twin density.

Besides brittle intergranular fracture, we find a quasi-brittle fracture mode of twin-free Ni_3Al accommodated by deformation twinning. The twinning partials keep on nucleating from the crack tip during loading, which facilitates the sharp crack propagation by leaving two free {111} surfaces. Whereas the pre-existing twin boundaries of nanotwinned Ni_3Al could effectively suppress the motion of emitted dislocations from crack tip. Dislocation avalanche or shear localization (depending on twin size) replaces deformation twinning as the dominating fracture mechanism in nanotwinned Ni_3Al. Thus crack blunting happens and results in ductile failure of the nanotwinned sample, as shown in Fig. 7.

The twin size effect on the fracture mode is further understood by a crack dislocation loop nucleation model and atomistic energetic analysis. The competition between twin boundary spacing and the critical size of dislocation nucleation results in a transition of fracture mechanisms in nanotwinned Ni_3Al. Energetics calculations indicate deformation twinning is much more difficult to take place in nanotwinned structure compared with twin-free counterpart. The twinnability becomes weaker when the twin is smaller. As a result, deformation twinning can no longer be served as a brittle fracture mechanism in nanotwinned Ni_3Al. Instead, avalanche-like dislocation nucleations in the vicinity of crack ductilize nanotwinned Ni_3Al.

To summarize, an atomic-level cracking model suggests nanotwinning as a possible pathway towards strengthening, toughening, and ductilizing Ni_3Al at the same time. The atomistic simulations agree with enhanced noticeable elongation and improved strength of Ni_3Al containing disordered lamellar nanotwins after HPT. Note that the disordered twin in experiment is different from the hypothesized real twin in the crack model and also in contrast with the pseudo-twinning found in MD. However, the versatile twin boundaries could play similar roles in terms of their interactions with dislocation nucleation and motion in nanostructures. Therefore, the present atomistic modellings can provide meaningful insight into the improved mechanical properties of the disordered nanotwinned Ni_3Al prepared via HPT. The promising insights from simulations suggest experimentalists to fabricate the real nanotwinned Ni_3Al, which could posses multiple excellent mechanical properties simultaneously. Since the coherent twin structure is thermally stable, the nanotwin technology is hypothesized to have minor influence on the thermal stability and high-temperature mechanical properties of Ni_3Al.

Finally, we note that environment embrittlement is a major causation of the intergranular fracture and the brittle nature of polycrystalline Ni_3Al. The present study is a primary effort to explore the intrinsic mechanical behavior of nanotwinned Ni_3Al. The atomistic simulations have not included a chemical effect on the fracture mechanism of the twin boundary in Ni_3Al. A further study including environment effect on cracking of both twin boundary and general grain boundary, such as reactive force field dynamics or DFT study, could partially clarify whether nanotwin is also strong against environmental embrittlement. Further calculations include the anisotropic effect, the interaction between conventional grain boundaries and twin boundary in the polycrystalline form, as well as corresponding experiments are required to further clarify the unique role of nanotwinning in brittle intermetallic alloys.

Acknowledgments

This work is financially supported by the NSFC (Nos. 11132011, 11402269, and 11472287), the National Key Basic Research Program of China (No. 2012CB937500), and the CAS/SAFEA International Partnership Program for Creative Research Teams.

Appendix A. Supplementary data

Supplementary data associated with this paper can be found in the online version at http://dx.doi.org/10.1016/j.msea.2015.10.006.

References

[1] R.C. Reed, The Superalloys: Fundamentals and Applications, Cambridge University Press, 2006.
[2] S.-Y. Wang, C.-Y. Wang, J.-H. Sun, W.-H. Duan, D.-L. Zhao, Energetics and electronic structure of Re and Ta in the γ' phase of Ni-based superalloys, Phys. Rev. B 65 (3) (2001) 035101, http://dx.doi.org/10.1103/PhysRevB.65.035101, URL ⟨http://link.aps.org/doi/10.1103/PhysRevB.65.035101⟩.
[3] C. Geng, C. Wang, T. Yu, Site preference and alloying effect of platinum group metals in γ' – Ni_3Al, Acta Mater. 52 (18) (2004) 5427–5433, http://dx.doi.org/10.1016/j.actamat.2004.08.007, URL ⟨http://linkinghub.elsevier.com/retrieve/pii/S1359645404004744⟩.

[4] Y.-J. Wang, C.-Y. Wang, A comparison of the ideal strength between $L1_2$ Co_3(Al, W) and Ni_3Al under tension and shear from first-principles calculations, Appl. Phys. Lett. 94 (26) (2009) 261909, http://dx.doi.org/10.1063/1.3170752, URL ⟨http://link.aip.org/link/APPLAB/v94/i26/p261909/s1&Agg=doi⟩.

[5] L. Kovarik, R. Unocic, J. Li, P. Sarosi, C. Shen, Y. Wang, M. Mills, Microtwinning and other shearing mechanisms at intermediate temperatures in Ni-based superalloys, Prog. Mater. Sci. 54 (6) (2009) 839–873, http://dx.doi.org/10.1016/j.pmatsci.2009.03.010, URL ⟨http://linkinghub.elsevier.com/retrieve/pii/S0079642509000139⟩.

[6] C.T. Liu, C.L. White, J.A. Horton, Effect of Boron on grain-boundaries in Ni_3Al, Acta Metall. 33 (2) (1985) 213–229, http://dx.doi.org/10.1016/0001-6160(85)90139-7, URL ⟨http://www.sciencedirect.com/science/article/pii/0001616085901397⟩.

[7] J.-Q. Su, M. Demura, T. Hirano, Grain-boundary fracture strength in Ni_3Al bicrystals, Philos. Mag. A 82 (8) (2002) 1541–1557, http://dx.doi.org/10.1080/01418610208240036, URL ⟨http://www.tandfonline.com/doi/abs/10.1080/01418610208240036⟩.

[8] E. George, C. Liu, D. Pope, Environmental embrittlement: the major cause of room-temperature brittleness in polycrystalline Ni_3Al, Scr. Metall. Mater. 27 (3) (1992) 365–370, http://dx.doi.org/10.1016/0956-716X(92)90527-L, URL ⟨http://www.sciencedirect.com/science/article/pii/0956716X9290527L⟩.

[9] M. Meyers, A. Mishra, D. Benson, Mechanical properties of nanocrystalline materials, Prog. Mater. Sci. 51 (4) (2006) 427–556, http://dx.doi.org/10.1016/j.pmatsci.2005.08.003, URL ⟨http://linkinghub.elsevier.com/retrieve/pii/S0079642505000447⟩.

[10] T. Zhu, J. Li, Ultra-strength materials, Prog. Mater. Sci. 55 (7) (2010) 710–757, http://dx.doi.org/10.1016/j.pmatsci.2010.04.001.

[11] L. Lu, Y. Shen, X. Chen, L. Qian, K. Lu, Ultrahigh strength and high electrical conductivity in copper, Science 304 (5669) (2004) 422–426, http://dx.doi.org/10.1126/science.1092905, URL ⟨http://www.ncbi.nlm.nih.gov/pubmed/15031435⟩.

[12] L. Lu, X. Chen, X. Huang, K. Lu, Revealing the maximum strength in nanotwinned copper, Science 323 (5914) (2009) 607–610, http://dx.doi.org/10.1126/science.1167641, URL ⟨http://www.ncbi.nlm.nih.gov/pubmed/19179523⟩.

[13] X. Li, Y. Wei, L. Lu, K. Lu, H. Gao, Dislocation nucleation governed softening and maximum strength in nano-twinned metals, Nature 464 (7290) (2010) 877–880, http://dx.doi.org/10.1038/nature08929, URL ⟨http://www.ncbi.nlm.nih.gov/pubmed/20376146⟩.

[14] Y. Zhu, X. Liao, X. Wu, Deformation twinning in nanocrystalline materials, Prog. Mater. Sci. 57 (1) (2012) 1–62, http://dx.doi.org/10.1016/j.pmatsci.2011.05.001, URL ⟨http://linkinghub.elsevier.com/retrieve/pii/S007964251100065X⟩.

[15] J.R. Greer, Nanotwinned metals: it's all about imperfections, Nat. Mater. 12 (8) (2013) 689–690, http://dx.doi.org/10.1038/nmat3721, URL ⟨http://www.nature.com/doifinder/10.1038/nmat3721⟩.

[16] Y. Wei, Y. Li, L. Zhu, Y. Liu, X. Lei, G. Wang, Y. Wu, Z. Mi, J. Liu, H. Wang, H. Gao, Evading the strength-ductility trade-off dilemma in steel through gradient hierarchical nanotwins, Nat. Commun. 5 (2014) 3580, http://dx.doi.org/10.1038/ncomms4580, URL ⟨http://www.pubmedcentral.nih.gov/articlerender.fcgi?artid=3988817&tool=pmcentrez&rendertype=abstract⟩.

[17] B. Gludovatz, A. Hohenwarter, D. Catoor, E.H. Chang, E.P. George, R.O. Ritchie, A fracture-resistant high-entropy alloy for cryogenic applications, Science 345 (6201) (2014) 1153, http://dx.doi.org/10.1126/science.1254581, URL ⟨http://www.sciencemag.org/content/345/6201/1153.short⟩.

[18] R.O. Ritchie, The conflicts between strength and toughness, Nat. Mater. 10 (11) (2011) 817–822, http://dx.doi.org/10.1038/nmat3115, URL ⟨http://www.nature.com/doifinder/10.1038/nmat3115⟩.

[19] T. Zhu, J. Li, A. Samanta, H.G. Kim, S. Suresh, Interfacial plasticity governs strain rate sensitivity and ductility in nanostructured metals, Proc. Natl. Acad. Sci. USA 104 (9) (2007) 3031–3036, http://dx.doi.org/10.1073/pnas.0611097104, URL ⟨http://www.pubmedcentral.nih.gov/articlerender.fcgi?artid=1805608&tool=pmcentrez&rendertype=abstract⟩.

[20] Y. Tian, B. Xu, D. Yu, Y. Ma, Y. Wang, Y. Jiang, W. Hu, C. Tang, Y. Gao, K. Luo, Z. Zhao, L.-M. Wang, B. Wen, J. He, Z. Liu, Ultrahard nanotwinned cubic boron nitride, Nature 493 (7432) (2013) 385–388, http://dx.doi.org/10.1038/nature11728, URL ⟨http://www.nature.com/doifinder/10.1038/nature11728⟩.

[21] Q. Huang, D. Yu, B. Xu, W. Hu, Y. Ma, Y. Wang, Z. Zhao, B. Wen, J. He, Z. Liu, Y. Tian, Nanotwinned diamond with unprecedented hardness and stability, Nature 510 (7504) (2014) 250–253, http://dx.doi.org/10.1038/nature13381, URL ⟨http://www.ncbi.nlm.nih.gov/pubmed/24919919⟩.

[22] J. Languillaume, F. Chmelik, G. Kapelski, F. Bordeaux, A. Nazarov, G. Canova, C. Esling, R. Valiev, B. Baudelet, Microstructures and hardness of ultrafine-grained Ni_3Al, Acta Metall. Mater. 41 (10) (1993) 2953–2962 http://dx.doi.org/10.1016/0956-7151(93)90110-E. URL ⟨http://www.sciencedirect.com/science/article/pii/095671519390110E⟩.

[23] A.V. Korznikov, G. Tram, O. Dimitrov, G.F. Korznikova, Z. Pakiela, The mechanism of nanocrystalline structure formation in Ni_3Al during severe plastic deformation, Acta Mater. 49 (2001) 663–671, http://dx.doi.org/10.1016/S1359-6454(00)00345-1, URL ⟨http://www.sciencedirect.com/science/article/pii/S1359645400003451⟩.

[24] C. Rentenberger, H. Karnthaler, On the evolution of a deformation induced nanostructure in a Ni_3Al alloy, Acta Mater. 53 (10) (2005) 3031–3040, http://dx.doi.org/10.1016/j.actamat.2005.03.016, URL ⟨http://linkinghub.elsevier.com/retrieve/pii/S1359645405001643⟩.

[25] O. Ciuca, K. Tsuchiya, Y. Yokoyama, Y. Todaka, M. Umemoto, Effect of nanocrystallization and twinning on hardness in Ni_3Al deformed by high-pressure torsion, Mater. Trans. 50 (5) (2009) 1123–1127, http://dx.doi.org/10.2320/matertrans.MRA2008485, URL ⟨http://joi.jlc.jst.go.jp/JST.JSTAGE/matertrans/MRA2008485?from=CrossRef⟩.

[26] O. Ciuca, K. Tsuchiya, Y. Yokoyama, Y. Todaka, M. Umemoto, Heterogeneous process of disordering and structural refinement in Ni3Al during severe plastic deformation by high-pressure torsion, Mater. Trans. 51 (1) (2010) 14–22, http://dx.doi.org/10.2320/matertrans.MB200915, URL ⟨http://joi.jlc.jst.go.jp/JST.JSTAGE/matertrans/MB200915?from=CrossRef⟩.

[27] K. Tsuchiya, O. Ciuca, Mechanical response of nanostructured intermetallics processed by high-pressure torsion straining, in: S. Fæster, N. Hansen, X. Huang, D.J. Jensen, B. Ralph (Eds.), Nanometals—Status and Perspective: Proceedings of the 33rd Risø International Symposium on Materials Science, Department of Wind Energy, Technical University of Denmark, 2012, pp. 129–141.

[28] R. Maaß, L. Meza, B. Gan, S. Tin, J.R. Greer, Ultrahigh strength of dislocation-free Ni_3Al nanocubes, Small 8 (12) (2012) 1869–1875, http://dx.doi.org/10.1002/smll.201102603, URL ⟨http://www.ncbi.nlm.nih.gov/pubmed/22454244⟩.

[29] S. Ogata, J. Li, S. Yip, Ideal pure shear strength of aluminum and copper, Science 298 (5594) (2002) 807–811, http://dx.doi.org/10.1126/science.1076652, URL ⟨http://www.ncbi.nlm.nih.gov/pubmed/12399585⟩.

[30] Y.-J. Wang, C.-Y. Wang, The alloying mechanisms of Re, Ru in the quaternary Ni-based superalloys γ/γ' interface: a first principles calculation, Mater. Sci. Eng. A 490 (1–2) (2008) 242–249, http://dx.doi.org/10.1016/j.msea.2008.01.023, URL ⟨http://linkinghub.elsevier.com/retrieve/pii/S0921509308000373⟩.

[31] X.-X. Yu, C.-Y. Wang, The effect of alloying elements on the dislocation climbing velocity in Ni: a first-principles study, Acta Mater. 57 (19) (2009) 5914–5920, http://dx.doi.org/10.1016/j.actamat.2009.08.019, URL ⟨http://linkinghub.elsevier.com/retrieve/pii/S1359645409005199⟩.

[32] X.-X. Yu, C.-Y. Wang, The effects of alloying elements on generalized stacking fault energies, strength and ductility of γ' – Ni^3Al, Mater. Sci. Eng. A 539 (2012) (2012) 38–41, http://dx.doi.org/10.1016/j.msea.2011.12.112, URL ⟨http://dx.doi.org/10.1016/j.msea.2011.12.112⟩.

[33] P. Zhang, L. Ma, F. Fan, Z. Zeng, C. Peng, P.E. Loya, Z. Liu, Y. Gong, J. Zhang, X. Zhang, P.M. Ajayan, T. Zhu, J. Lou, Fracture toughness of graphene, Nat. Commun. 5 (2014) 3782, http://dx.doi.org/10.1038/ncomms4782, URL ⟨http://www.ncbi.nlm.nih.gov/pubmed/24777167⟩.

[34] D. Jang, X. Li, H. Gao, J.R. Greer, Deformation mechanisms in nanotwinned metal nanopillars, Nat. Nanotechnol. 7 (9) (2012) 594–601, http://dx.doi.org/10.1038/nnano.2012.116.

[35] Y. Zhong, K. Gall, T. Zhu, Atomistic characterization of pseudoelasticity and shape memory in NiTi nanopillars, Acta Mater. 60 (18) (2012) 6301–6311, http://dx.doi.org/10.1016/j.actamat.2012.08.004, URL ⟨http://linkinghub.elsevier.com/retrieve/pii/S1359645412005332⟩.

[36] Z. You, X. Li, L. Gui, Q. Lu, T. Zhu, H. Gao, L. Lu, Plastic anisotropy and associated deformation mechanisms in nanotwinned metals, Acta Mater. 61 (1) (2013) 217–227, http://dx.doi.org/10.1016/j.actamat.2012.09.052, URL ⟨http://linkinghub.elsevier.com/retrieve/pii/S1359645412006854⟩.

[37] E. Bitzek, P. Gumbsch, Mechanisms of dislocation multiplication at crack tips, Acta Mater. 61 (4) (2013) 1394–1403, http://dx.doi.org/10.1016/j.actamat.2012.11.016, URL ⟨http://linkinghub.elsevier.com/retrieve/pii/S1359645412008208⟩.

[38] J.J. Mo, E. Bitzek, Fracture toughness and bond trapping of grain boundary cracks, Acta Mater. 73 (2014) 1–11, http://dx.doi.org/10.1016/j.actamat.2014.03.035, URL ⟨http://www.sciencedirect.com/science/article/pii/S1359645414001827⟩.

[39] J. Amodeo, C. Begau, E. Bitzek, Atomistic simulations of compression tests on Ni_3Al nanocubes, Mater. Res. Lett. 2 (3) (2014) 140–145, http://dx.doi.org/10.1080/21663831.2013.878884, URL ⟨http://www.tandfonline.com/doi/abs/10.1080/21663831.2013.878884⟩.

[40] Y.-J. Wang, G.-J.J. Gao, S. Ogata, Size-dependent transition of deformation mechanism, and nonlinear elasticity in Ni_3Al nanowires, Appl. Phys. Lett. 102 (4) (2013) 041902, http://dx.doi.org/10.1063/1.4789528, URL ⟨http://link.aip.org/link/APPLAB/v102/i4/p041902/s1&Agg=doi⟩.

[41] Y. Mishin, Atomistic modeling of the γ and γ' – phases of the Ni–Al system, Acta Mater. 52 (6) (2004) 1451–1467, http://dx.doi.org/10.1016/j.actamat.2003.11.026, URL ⟨http://linkinghub.elsevier.com/retrieve/pii/S1359645403007262⟩.

[42] M.L. Falk, Molecular-dynamics study of ductile and brittle fracture in model noncrystalline solids, Phys. Rev. B 60 (10) (1999) 7062–7070, http://dx.doi.org/10.1017/CBO9781107415324.004, URL ⟨http://journals.aps.org/prb/abstract/10.1103/PhysRevB.60.7062⟩.

[43] K. Leung, Z. Pan, D. Warner, Atomistic-based predictions of crack tip behavior in silicon carbide across a range of temperatures and strain rates, Acta Mater. 77 (2014) 324–334, http://dx.doi.org/10.1016/j.actamat.2014.06.016, URL ⟨http://linkinghub.elsevier.com/retrieve/pii/S1359645414004364⟩.

[44] F. Yuan, L. Huang, Brittle to ductile transition in densified silica glass, Sci. Rep. 4 (2014) 5035, http://dx.doi.org/10.1038/srep05035, URL ⟨http://apps.webofknowledge.com/full_record.do?product=UA&search_mode=GeneralSearch&qid=9&SID=1ENpGxMnuVUc2EAE3Eb&page=2&doc=18⟩.

[45] Y. Shi, J. Luo, F. Yuan, L. Huang, Intrinsic ductility of glassy solids, J. Appl. Phys. 115 (4) (2014) 043528, http://dx.doi.org/10.1063/1.4862959, URL ⟨http://scitation.aip.org/content/aip/journal/jap/115/4/10.1063/1.4862959⟩.

[46] S. Plimpton, Fast parallel algorithms for short-range molecular dynamics, J.

Comput. Phys. 117 (1) (1995) 1–19, http://dx.doi.org/10.1006/jcph.1995.1039.
[47] S. Nosé, A molecular dynamics method for simulations in the canonical ensemble, Mol. Phys. 52 (2) (1984) 255–268, http://dx.doi.org/10.1080/00268978400101201 arXiv:http://dx.doi.org/10.1080/00268978400101201.
[48] W. Hoover, Canonical dynamics: equilibrium phase-space distributions, Phys. Rev. A 31 (1985) 1695–1697, http://dx.doi.org/10.1103/PhysRevA.31.1695, URL ⟨http://link.aps.org/doi/10.1103/PhysRevA.31.1695⟩.
[49] M. Parrinello, Polymorphic transitions in single crystals: a new molecular dynamics method, J. Appl. Phys. 52 (12) (1981) 7182, http://dx.doi.org/10.1063/1.328693, URL ⟨http://scitation.aip.org/content/aip/journal/jap/52/12/10.1063/1.328693⟩.
[50] A. Stukowski, Visualization and analysis of atomistic simulation data with OVITO-the Open Visualization Tool, Model. Simul. Mater. Sci. Eng. 18 (1) (2010) 015012, http://dx.doi.org/10.1088/0965-0393/18/1/015012, URL ⟨http://stacks.iop.org/0965-0393/18/i=1/a=015012?key=crossref.6895e2c3bb522d1563fb2e2fe9f22789⟩.
[51] J. Li, AtomEye: an efficient atomistic configuration viewer, Model. Simul. Mater. Sci. Eng. 11 (2) (2003) 173–177, http://dx.doi.org/10.1088/0965-0393/11/2/305, URL ⟨http://stacks.iop.org/0965-0393/11/i=2/a=305?key=crossref.4195f4cb7374ee2ac984c1de585d8869⟩.
[52] A.A. Griffith, The phenomena of rupture and flow in solids, Philos. Trans. R. Soc. Lond. A 221 (1921) 163–198, http://dx.doi.org/10.1098/rsta.1921.0006, URL ⟨http://rsta.royalsocietypublishing.org/content/221/582-593/163⟩.
[53] J.D. Rigney, J.J. Lewandowski, Fracture toughness of monolithic nickel aluminide intermetallics, Mater. Sci. Eng. A 149 (2) (1992) 143–151, http://dx.doi.org/10.1016/0921-5093(92)90375-B, URL ⟨http://linkinghub.elsevier.com/retrieve/pii/092150939290375B⟩.
[54] Y. Liu, Z. Xie, Twinning and detwinning of ⟨011⟩ type II twin in shape memory alloy, Acta Mater. 51 (18) (2003) 5529–5543, http://dx.doi.org/10.1016/S1359-6454(03)00417-8.
[55] T. Ezaz, H. Sehitoglu, H.J. Maier, Energetics of (1 1 4) twinning in B2 NiTi under coupled shear and shuffle, Acta Mater. 60 (1) (2012) 339–348, http://dx.doi.org/10.1016/j.actamat.2011.09.032.
[56] T. Zhu, J. Li, S. Yip, Atomistic study of dislocation loop emission from a crack tip, Phys. Rev. Lett. 93 (2) (2004) 025503, http://dx.doi.org/10.1103/PhysRevLett.93.025503, URL ⟨http://link.aps.org/doi/10.1103/PhysRevLett.93.025503⟩.